

An N -Body Solver for Square Root Iteration

Matt Challacombe,* Terry Haut,[†] and Nicolas Bock[‡]

Theoretical Division, Los Alamos National Laboratory

We develop the Sparse Approximate Matrix Multiply n -body solver for first order Newton Schulz iteration of the matrix square root and inverse square root. The solver performs an n -body occlusion-cull, yeilding a bounded relative error in the matrix-matrix product and reduced complexity for problems with structured metric decay. This complexity reduction cooresponds to the hierarchical resolution of algebraic structures within recursive volume of the product, a consequence of metric locality. For square root iteration, strongly localized sub-volumes are culled about plane-diagonals and along the cube-diagonal, cooresponding to resolution of the identity.

The main contributions of this paper are bounds on the SpAMM product and demonstration of a new algebraic locality that develops in these sub-volumes with strongly contractive identity iteration. This contraction cooresponds to the deflation of sub-volumes onto plane diagonals of the resolvent, and to a stronger bound on the SpAMM product.

Also, we carry out a first order Fréchet analyses for single and dual channel instances of the square root iteration, and look at bifurcations due to ill-conditioning and a too-agresive SpAMM approximation. Then, we show that extreme SpAMM approximations and strongly contractive identity iteration can be achieved through iterated regularization, and demonstrate the potential for orders of magnitude acceleration with product representation of the inverse factor.

I. INTRODUCTION

In many areas of application, long range, high value correlations lead to matrix equations with decay properties. By decay, we mean an approximate inverse relationship between matrix elements and an associated distance; this may be a simple inverse relationship between matrix elements and the Cartesian distance between corresponding support functions, or it may involve a non-Euclidean distance, *e.g.* a generalized measure between character strings in a training library [].

Matrix equations with decay have history and recent development in the statistics and statistical physics literature [1–5]. Also recently, methods for meshfree interpolation are demonstrating remarkable predictive power through delocalized correlations and cooresponding ill-conditioned matrix equations with extreme slow decay [], a problem equivalent to the LCAO Gaussian basis problem in quantum chemistry []. Generally, local support functions are correlated through Lowdin’s symmetric orthogonalization based on the matrix inverse square root [6, 7], yeilding representation independent matrix equations. In electronic structure, important long-range correlations manifest in slow decay properties of the gap shifted matrix sign function, as projector of the effective Hamiltonian (Fig. I). Both of these matrix problem with decay, the matrix sign function and the matrix inverse

square root, are related by Higham’s identity:

$$\text{sign} \left(\begin{bmatrix} 0 & s \\ I & 0 \end{bmatrix} \right) = \begin{bmatrix} 0 & s^{1/2} \\ s^{-1/2} & 0 \end{bmatrix}. \quad (1)$$

The theory and computation of these matrix functions is given in Higham’s reference [8].

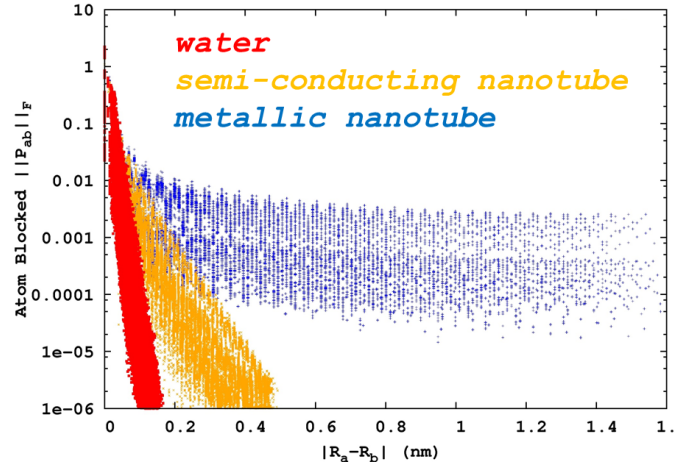


FIG. 1: Examples from electronic structure of decay for the spectral projector (gap shifted sign function) with respect to local (atomic) support. Shown is decay for systems with correlations that are short (insulating water), medium (semi-conducting 4,3 nanotube), and long (metallic 3,3 nanotube) ranged, from exponential (insulating) to algebraic (metallic).

*Electronic address: matt.challacombe@freeon.org; URL: <http://www.freeon.org>

[†]Electronic address: haut@lanl.gov

[‡]Electronic address: nicolasbock@freeon.org; URL: <http://www.freeon.org>

A well conditioned matrix s may often correspond to matrix sign and inverse square root functions with rapid exponential decay, and be amenable to *ad hoc* matrix truncation or “sparsification”, $\bar{s} = s + \epsilon_\tau^s$, where ϵ_τ^s is the error introduced according to some criterion τ . The criterion τ might be a drop-tolerance, $\epsilon_\tau^s = \{-s_{ij} * \hat{e}_i | |s_{ij}| <$

$\tau\}$, a radial cutoff, $\epsilon_\tau^s = \{-s_{ij} * \hat{\mathbf{e}}_i \mid \|\mathbf{r}_i - \mathbf{r}_j\| > \tau\}$, or some other approach to truncation, perhaps involving a sparsity pattern chosen *a priori* for computational expedience. Then, the sparse general matrix-matrix multiply (**SpGEMM**) [9–12] may be employed, yielding fast solutions for multiplication rich iterations with fill-in modulated by truncation. Comprehensive surveys of these methods in the numerical linear algebra are given by Benzi [13, 14], and by Bowler [15] and Benzi [16] for electronic structure.

Often however, matrix truncation is ineffective for ill-conditioned problems, because of slow decay, and because of increased numerical sensitivities to poorly controled (absolute) truncation errors, *e.g.* in the matrix-product:

$$\overline{\mathbf{a} \cdot \mathbf{b}} = \mathbf{a} \cdot \mathbf{b} + \epsilon_\tau^a \cdot \mathbf{b} + \mathbf{a} \cdot \epsilon_\tau^b + \mathcal{O}(\tau^2). \quad (2)$$

An alterative approach is to find a reduced rank approximation closed under the opperations of interest [?]. However, compression to a reduced rank may be expensive if the rank is not much much smaller than the dimension. Both of these methods, truncation and rank reduction, are focused on matrix data as the target for compresion. In this contribution, our target for compression is instead the matrix product itself. For problems with decay, we show that an underlying metric locality, together with a new form of algebraic locality, can lead to complexity reduction under contractive iteration and the n -body occlusion-cull. The organization of this paper follows.

Contents

I. Introduction	1
II. SpAMM	2
A. Occlusion-cull	2
B. Bound	3
C. Related research	3
III. First Order Newton-Shulz Iteration	4
A. Sign iteration	4
B. Square root iteration	4
C. Mapping	5
IV. Error Flows in Square Root Iteration	5
A. Stability	5
B. Fréchet derivatives	5
C. Displacements	5
D. Most approximate but still stable	6
V. Regularization	7
A. Product representation	7
B. Effective by one order	7

C. Iterative regularization	7
VI. Locality	9
A. Spatial, metric and temporal locality	9
B. Algebraic locality	9
C. Complexity reduction	9
VII. Conclusions	9
A. Implementation	11
B. Data	11
References	11

II. SpAMM

In this contribution, we consider an N -body approach to the approximation of matrix functions with decay, based on the quadtree data structure [? ?]

$$\mathbf{a}^i = \begin{bmatrix} \mathbf{a}_{00}^{i+1} & \mathbf{a}_{01}^{i+1} \\ \mathbf{a}_{10}^{i+1} & \mathbf{a}_{11}^{i+1} \end{bmatrix}, \quad (3)$$

and orderings that are locality preserving []. Orderings that preserve data locality are well developed and *generic* in the database theory [], providing fast spatial and metric queries. Locality enabled, fast data access is central to b -body approximations [], and an important problem for enterprise [] and runtime systems [], moreso with memory hierarchies becoming increasingly asynchronous and decentralized [?]. For matrices with decay, orderings that preserve locality lead to blocked-by-magnitude matrix structures with well segregated neighborhoods, inhabited by matrix elements of like size, and efficiently resolved by the quadtree data structure [].

A. Occlusion-cull

The Sparse Approximate Matrix Multiply (**SpAMM**) carries out occlusion-culling to find only the most important sub-volumes in an approximate matrix product. **SpAMM** has evolved from a row-column oriented skipout mechanism within the BCSR and DBCSR structures [], to hierarchical approaches based on the quadtree and related to the occlusion-culling found in advanced mechanics and graphics methodologies [], with occlusion the avoidance of unessesary tree-work and culling the collection of significant tasks. Here, we ammend the **SpAMM** occlusion-cull with the recursion:

$$\mathbf{a}^i \otimes_{\tau} \mathbf{b}^i = \begin{cases} \emptyset & \text{if } \|\mathbf{a}^i\| \|\mathbf{b}^i\| < \tau \|\mathbf{a}\| \|\mathbf{b}\| \\ \mathbf{a}^i \cdot \mathbf{b}^i & \text{if } (\mathbf{i} = \text{leaf}) \\ \left[\mathbf{a}_{00}^{i+1} \otimes_{\tau} \mathbf{b}_{00}^{i+1} + \mathbf{a}_{01}^{i+1} \otimes_{\tau} \mathbf{b}_{10}^{i+1}, \quad \mathbf{a}_{00}^{i+1} \otimes_{\tau} \mathbf{b}_{01}^{i+1} + \mathbf{a}_{01}^{i+1} \otimes_{\tau} \mathbf{b}_{11}^{i+1} \right] & \text{else} \\ \left[\mathbf{a}_{00}^{i+1} \otimes_{\tau} \mathbf{b}_{01}^{i+1} + \mathbf{a}_{01}^{i+1} \otimes_{\tau} \mathbf{b}_{11}^{i+1}, \quad \mathbf{a}_{00}^{i+1} \otimes_{\tau} \mathbf{b}_{01}^{i+1} + \mathbf{a}_{01}^{i+1} \otimes_{\tau} \mathbf{b}_{11}^{i+1} \right] & \text{else} \end{cases}, \quad (4)$$

which bounds the relative occlusion error

$$\frac{\|\Delta_{\tau}^{a \cdot b}\|}{n^2} \leq \tau \|\mathbf{a}\| \|\mathbf{b}\|, \quad (5)$$

that occurs in the approximate product

$$\widetilde{\mathbf{a} \cdot \mathbf{b}} \equiv \mathbf{a} \otimes_{\tau} \mathbf{b} = \mathbf{a} \cdot \mathbf{b} + \Delta_{\tau}^{a \cdot b}, \quad (6)$$

where $\|\cdot\| \equiv \|\cdot\|_F$ is a sub-multiplicative norm $\|\cdot\|$.

B. Bound

We now prove (5).

Proposition 1. Let $\tau_{A,B} = \tau \|\mathbf{A}\| \|\mathbf{B}\|$. Then for each i,j ,

$$\left| (A \otimes_{\tau} B)_{ij} - (A \cdot B)_{ij} \right| \leq n \tau_{A,B},$$

and

$$\|A \otimes_{\tau} B - A \cdot B\|_F \leq n^2 \tau_{A,B}.$$

Proof. We first show the following technical result: it is possible to choose $\alpha_{lij} \in \{0, 1\}$ such that

$$(A \otimes_{\tau} B)_{ij} = \sum_{l=1}^n A_{il} B_{lj} \alpha_{lij}, \quad (7)$$

In addition, if $\alpha_{lij} = 0$, then $|A_{il}| |B_{lj}| < \tau_{A,B}$. To show this, we use induction on the number k_{\max} of levels.

First, if $k_{\max} = 0$,

$$A \otimes_{\tau} B = \begin{cases} 0 & \text{if } \|A\|_F \|B\|_F < \tau_{A,B}, \\ A \cdot B & \text{else.} \end{cases}$$

Therefore, $A \otimes_{\tau} B$ is of the form (7) with either all $\alpha_{lij} = 0$ or all $\alpha_{lij} = 1$. Moreover, if $\alpha_{lij} = 0$, then $|A_{il}| |B_{lj}| \leq \|A\|_F \|B\|_F < \tau_{A,B}$.

Now assume that the claim holds for $k_{\max} - 1$. We show that it holds for k_{\max} . Indeed, if $\|A\|_F \|B\|_F < \tau_{A,B}$, we have that $A \otimes_{\tau} B = 0$, which is of the form (7) with all $\alpha_{lij} = 0$. Also, if $\alpha_{lij} = 0$, then $|A_{il}| |B_{lj}| < \|A\|_F \|B\|_F < \tau_{A,B}$.

Now assume that $\|A\|_F \|B\|_F \geq \tau_{A,B}$. Then

$$A \otimes_{\tau} B = \begin{pmatrix} A_{11} \otimes_{\tau} B_{11} + A_{12} \otimes_{\tau} B_{21} & A_{11} \otimes_{\tau} B_{12} + A_{12} \otimes_{\tau} B_{22} \\ A_{21} \otimes_{\tau} B_{11} + A_{22} \otimes_{\tau} B_{21} & A_{21} \otimes_{\tau} B_{12} + A_{22} \otimes_{\tau} B_{22} \end{pmatrix}.$$

We need to consider four cases: $i \leq n/2$ and $j \leq n/2$, $i > n/2$ and $j > n/2$, $i > n/2$ and $j \leq n/2$, and, finally, $i > n/2$ and $j > n/2$. Since the analysis is similar for all four cases, we only consider $i \leq n/2$ and $j \leq n/2$. We have that

$$\begin{aligned} (A \otimes_{\tau} B)_{ij} &= (A_{11} \otimes_{\tau} B_{11} + A_{12} \otimes_{\tau} B_{21})_{ij} \\ &= \sum_{l=1}^{n/2} (A_{11})_{il} (B_{11})_{lj} \alpha_{lij}^{(1)} + \\ &\quad \sum_{l=1}^{n/2} (A_{12})_{il} (B_{21})_{lj} \alpha_{lij}^{(2)} \\ &= \sum_{l=1}^n A_{il} B_{lj} \alpha_{lij}, \end{aligned}$$

where we used the induction hypothesis in the second equality.

Now suppose that $\alpha_{lij} = 0$ for some l . Then $\tilde{\alpha}_{lij}^{(1)} = 0$ if $l \leq n/2$ or $\tilde{\alpha}_{l-n/2,ij}^{(2)} = 0$ if $l > n/2$. If, e.g., $\tilde{\alpha}_{l-n/2,ij}^{(2)} = 0$, then $|A_{il}| |B_{lj}| = |(A_{12})_{i,l-n/2}| |(B_{21})_{l-n/2,j}| < \tau_{A,B}$, where we used the induction hypothesis in the final inequality. The analysis for $l \leq n/2$ is similar, and the claim follows.

We can now finish the proof of Proposition 1. Indeed, by (7),

$$\begin{aligned} \left| (A \otimes_{\tau} B)_{ij} - (A \cdot B)_{ij} \right| &\leq \sum_{l=1}^n |A_{il} B_{lj}| |\alpha_{lij} - 1| \\ &= \sum_{\alpha_{lij}=0} |A_{il} B_{lj}|. \end{aligned}$$

In addition, if $\alpha_{lij} = 0$, then $|A_{il} B_{lj}| < \tau_{A,B}$ and the lemma follows. \square

C. Related research

SpAMM is perhaps most closely related to the Strassen-like branch of fast matrix multiplication [17, 18]. In

the Strassen-like approach, disjoint volumes in (abstract) tensor intermediates are omitted recursively [1]. In the SpAMM approach to fast multixplication, the numerically most significant volumes in naïve (ijk) tensor intermediates are culled, with error bounded by Eq. (5). This bound makes \otimes_τ a *stable* form of fast multiplication, as explained by Demmel, Dumitriu and Holz (DDH; Ref. [7]).

SpAMM is a n -body method for fast matrix multiplication, related to the generalized methods popularized by Grey [19, 20]. In our development, generalization reflects the *genericity* [1] of recursive data access [1], enabling range queries, metric queries, higher dimensional queries and so on, with common frameworks, structures and runtimes. So far, we have prototyped n -body solvers for mainstay problems in modern electronic structure theory [7, 8], involving Fock exchange [1], semi-local exchange-correlation functionals [1], the Hartree (Coulomb) interaction [1], matrix sign function [1] and the matrix inverse square root (this work). This contribution is cornerstone for the simplification and evolution of these solvers.

Top-down n -body recursion and breadth-first map-reduction may be viewed as two sides of the same problem [7]. Emergent data frameworks and functional programming languages that support generic recursion and map skelitizations may enable early exploitation of commodity (decentralized) concurrence by scientific n -body solvers, as well as software sustainability [7]. For centralized, distributed architectures, n -body methods offer well established protocols for turning spatial and metric locality into data and temporal locality [1]. Recently, Driscoll *et. al* showed perfect strong scaling and communication optimality for pairwise n -body methods [7]. Bridging the gap between n -body solver and fast matrix multiplication, we recently demonstrated strong scaling for fast matrix multiplication (SpAMM) [1].

This work offers a data local alternative to fast non-deterministic methods for sampling the product, which include sketching [21–26], joining [27–33], sensing [1] and probing [1]. These methods involve a weighted (probabilistic) and on the fly sampling, with the potential for complexity reduction in the case of random distributions. SpAMM also employs on the fly weighted sampling, but with compression through locality, brought about by algebraic correlations (towards identity) and also in the metric structure, through strong Euclidean locality.

Finally, previous work on the scaled NS iteration has heavily influenced this work. Formost is Higham, Mackey, Mackey and T (HMMT; Ref. [1]) masterwork on convergence of NS iteration under all groups, wherein HMMT also develop Fréchet analyses for single square root iteration at the fixed point. Also, important inspiration comes from Chen and Chow's [1] approach to scaled NS iteration for ill-conditioned problems [1], and from the Helgaker groups work on NS iteration, whose notation we follow in part [1].

III. FIRST ORDER NEWTON-SHULZ ITERATION

There are two common, first order NS iterations; the sign iteration and the square root iteration, related by the square, $\mathbf{I}(\cdot) = \text{sign}^2(\cdot)$. These equivalent iterations converge linearly at first, then enter a basin of stability marked by super-linear convergence.

A. Sign iteration

For the NS sign iteration, this basin is marked by a behavioral change in the difference $\delta\mathbf{X}_k = \widetilde{\mathbf{X}}_k - \mathbf{X}_k = \text{sign}(\mathbf{X}_{k-1} + \delta\mathbf{X}_{k-1}) - \text{sign}(\mathbf{X}_{k-1})$, where $\delta\mathbf{X}_{k-1}$ is some previous error. The change in behavior is associated with the onset of idempotence and the bounded eigenvalues of $\text{sign}'(\cdot)$, leading to stable iteration when $\text{sign}'(\mathbf{X}_{k-1}) \delta\mathbf{X}_{k-1} < 1$. Global perturbative bounds on this iteration have been derived by Bai and Demmel [34], while Byers, He and Mehrmann [1] developed asymptotic bounds. The automatic stability of sign iteration is a well developed theme in Ref.[8].

B. Square root iteration

In this work, we are concerned with resolution of the identity [1]

$$\mathbf{I}(s) = s^{1/2} \cdot s^{-1/2}, \quad (8)$$

and its low-complexity computation with fast methods.

Starting with eigenvalues rescaled to the domain $(0, 1]$ with the easily obtained largest eigenvalue, $s \leftarrow s/s_{N-1}$, and with $\mathbf{z}_0 = \mathbf{I}$ and $\mathbf{x}_0 = \mathbf{y}_0 = s$, the cooresponding canonical, “dual” channel square root iteration is:

$$\text{Then, using } h_\alpha[\tilde{\mathbf{x}}_{k-2}] = h_\alpha[\mathbf{x}_{k-2}] + h'_\alpha \delta\mathbf{x}_{k-2} \quad (10)$$

$\mathbf{y}_k \leftarrow h_\alpha[\mathbf{y}_{k-1} \cdot \mathbf{z}_{k-1}] \cdot \mathbf{y}_{k-1}$
 $\mathbf{z}_k \leftarrow \mathbf{z}_{k-1} \cdot h_\alpha[\mathbf{y}_{k-1} \cdot \mathbf{z}_{k-1}]$, converging as $\mathbf{y}_k \rightarrow s^{1/2}$,
 $\mathbf{z}_k \rightarrow s^{-1/2}$ and $\mathbf{x}_k \rightarrow \mathbf{I}$, with eigenvalues aggregated towards 0 or 1 by the NS map $h_\alpha[\mathbf{x}] = \frac{\sqrt{\alpha}}{2}(3 - \alpha\mathbf{x})$ [1]. As in the case of sign iteration, this cannonical iteration was shown by Higham, Mackey, Mackey and Tisseur [35] to remain strongly bounded in the superlinear regime, by idempotent Frechet derivatives about the fixed point $(s^{1/2}, s^{-1/2})$, in the direction $(\delta\mathbf{y}_{k-1}, \delta\mathbf{z}_{k-1})$:

$$\delta\mathbf{y}_k = \frac{1}{2}\delta\mathbf{y}_{k-1} - \frac{1}{2}s^{1/2} \cdot \delta\mathbf{z}_{k-1} \cdot s^{1/2} \quad (10)$$

$$\delta\mathbf{z}_k = \frac{1}{2}\delta\mathbf{z}_{k-1} - \frac{1}{2}s^{-1/2} \cdot \delta\mathbf{y}_{k-1} \cdot s^{-1/2}. \quad (11)$$

In addition to the dual channel instance, we also consider the “single” Then, using

$$h_\alpha[\tilde{\mathbf{x}}_{k-2}] = h_\alpha[\mathbf{x}_{k-2}] + h'_\alpha \delta\mathbf{x}_{k-2} \quad (12)$$

channel version of square root iteration,

$$\begin{aligned} \mathbf{z}_k &\leftarrow \mathbf{z}_{k-1} \cdot h_\alpha [\mathbf{x}_{k-1}] , \\ \mathbf{x}_k &\leftarrow \mathbf{z}_k^\dagger \cdot \mathbf{s} \cdot \mathbf{z}_k . \end{aligned} \quad (13)$$

C. Mapping

The NS logistic map for the square root iteration is $h_\alpha[\mathbf{x}] = \frac{\sqrt{\alpha}}{2}(3 - \alpha\mathbf{x})$, with the initial rate of convergence controlled by h'_α and the smallest eigenvalue, x_0 . Various schemes for controlling the values α towards convergence, notably by Pan and Schreiber [37], and more recently, Jie and Chen [36], who demonstrated $2\times$ acceleration for very ill-conditioned problems with their new scaling approach.

In addition to scaling of the NS logistic, we introduce a stabilizing map that accounts for eigenvalues tossed out of bounds by \otimes_τ . This stabilization is the transformation $[0, 1] \rightarrow [0 + \varepsilon, 1 - \varepsilon]$ (shift and scale), carried out prior to application of the logistic.

The most important aspect of these scaling and stabilization maps is to turn them off towards convergence. Conventional methods often compute a lowest eigenvalue to monitor convergence [36, 37], but this may be too expensive for ill-conditioned problems. Alternatively, we monitor convergence simply with the relative trace error, $t_k = (n - \text{tr } \tilde{\mathbf{x}}_k) n^{-1}$. Then, empirically developed sigmoidal functions are used to damp the scaling parameter to unity,

$$\alpha(t) = 1. + 1.85 \times \left(1 + e^{-50.(t-.35)}\right)^{-1}$$

and the stability parameter to zero,

$$\varepsilon(t) = .1 \times \left(1 + e^{-75.(t-.30)}\right)^{-1}. \quad (15)$$

These functions are used throughout.

IV. ERROR FLOWS IN SQUARE ROOT ITERATION

A. Stability

Stability in the square root iteration is determined by the differential

$$\delta\mathbf{x}_k = \mathbf{x}_{\delta\hat{\mathbf{y}}_{k-1}} \times \delta\mathbf{y}_{k-1} + \mathbf{x}_{\delta\hat{\mathbf{z}}_{k-1}} \times \delta\mathbf{z}_{k-1} + \mathcal{O}(\tau^2) \quad (16)$$

which must remain bounded below one to avoid divergence. The corresponding Fréchet derivatives are

$$\mathbf{x}_{\delta\hat{\mathbf{y}}_{k-1}} = \lim_{\tau \rightarrow 0} \frac{\mathbf{x}(\mathbf{y}_{k-1} + \tau\delta\hat{\mathbf{y}}_{k-1}, \mathbf{z}_{k-1}) - \mathbf{x}_k}{\tau} \quad (17)$$

and

$$\mathbf{x}_{\delta\hat{\mathbf{z}}_{k-1}} = \lim_{\tau \rightarrow 0} \frac{\mathbf{x}(\mathbf{y}_{k-1}, \mathbf{z}_{k-1} + \tau\delta\hat{\mathbf{z}}_{k-1}) - \mathbf{x}_k}{\tau}, \quad (18)$$

along unit directions of the previous errors $\delta\hat{\mathbf{y}}_{k-1}$ and $\delta\hat{\mathbf{z}}_{k-1}$, by an amount determined by the displacements $\delta\mathbf{y}_{k-1} = \|\delta\mathbf{y}_{k-1}\|$ and $\delta\mathbf{z}_{k-1} = \|\delta\mathbf{z}_{k-1}\|$. In the single instance, we have simply:

$$\delta\mathbf{x}_k = \mathbf{x}_{\delta\hat{\mathbf{z}}_{k-1}} \times \delta\mathbf{z}_{k-1} + \mathcal{O}(\tau^2). \quad (19)$$

This formulation makes plain changes about the solvent, separating orientational effects of the directional derivatives, set mostly by the underlying exact linear algebra, from changes to error displacements, which involve both the action of derivatives on previous errors, as well as the SpAMM occlusion errors local to the product.

B. Fréchet derivatives

In the dual instance, Fréchet derivatives occurring in Eq. (16) are:

$$\begin{aligned} \mathbf{x}_{\delta\hat{\mathbf{z}}_{k-1}} &= \mathbf{y}_{k-1} \cdot h'_\alpha \delta\hat{\mathbf{z}}_{k-1} \cdot \mathbf{y}_{k-1} \cdot \mathbf{z}_k \\ &\quad + \mathbf{y}_k \cdot \delta\hat{\mathbf{z}}_{k-1} \cdot h_\alpha [\mathbf{x}_{k-1}] \\ &\quad + \mathbf{y}_k \cdot \mathbf{z}_{k-1} \cdot \mathbf{y}_{k-1} \cdot h'_\alpha \delta\hat{\mathbf{z}}_{k-1}, \end{aligned} \quad (20)$$

and

$$\begin{aligned} \mathbf{x}_{\delta\hat{\mathbf{y}}_{k-1}} &= h_\alpha [\mathbf{x}_{k-1}] \cdot \delta\hat{\mathbf{y}}_{k-1} \cdot \mathbf{z}_k \\ &\quad + h'_\alpha \delta\hat{\mathbf{y}}_{k-1} \cdot \mathbf{z}_{k-1} \cdot \mathbf{y}_{k-1} \cdot \mathbf{z}_k \\ &\quad + \mathbf{y}_k \cdot \mathbf{z}_{k-1} \cdot h'_\alpha \delta\hat{\mathbf{y}}_{k-1} \cdot \mathbf{z}_{k-1}. \end{aligned} \quad (21)$$

Closer to the fixed point orbit, $\mathbf{y}_k \cdot \mathbf{z}_{k-1} \rightarrow \mathbf{I}$, $\mathbf{y}_{k-1} \cdot \mathbf{z}_k \rightarrow \mathbf{I}$, $h_\alpha [\mathbf{x}_k] \rightarrow \mathbf{I}$ and $h'_\alpha \rightarrow -\frac{1}{2}$ [?]. Then,

$$\mathbf{x}_{\delta\hat{\mathbf{y}}_{k-1}} \rightarrow \delta\hat{\mathbf{y}}_{k-1} \cdot (\mathbf{z}_k - \mathbf{z}_{k-1}) \quad (22)$$

and

$$\mathbf{x}_{\delta\hat{\mathbf{z}}_{k-1}} \rightarrow (\mathbf{y}_k - \mathbf{y}_{k-1}) \cdot \delta\hat{\mathbf{z}}_{k-1}. \quad (23)$$

Likewise, in the single channel instance:

$$\begin{aligned} \mathbf{x}_{\hat{\mathbf{z}}_{k-1}} &\rightarrow (\mathbf{z}_k - \mathbf{z}_{k-1})^\dagger \cdot \mathbf{s} \cdot \delta\hat{\mathbf{z}}_{k-1} \\ &\quad + \delta\hat{\mathbf{z}}_{k-1}^\dagger \cdot \mathbf{s} \cdot (\mathbf{z}_k - \mathbf{z}_{k-1}). \end{aligned} \quad (24)$$

About the fixed point then, error flow in the \mathbf{y}_k and the \mathbf{z}_k channels is tightly quenched, corresponding to $\mathbf{x}_{\delta\hat{\mathbf{x}}_{k-1}} \rightarrow \mathbf{I}$ and identity iteration [?].

C. Displacements

Countering orientational convergence, determined almost entirely by the underlying exact iterations, is the the compounding displacement error, determined by SpAMM occlusion in each of three products, at each step, and

also involving previous errors. Here, we look at just the displacement δz_{k-1} , which has the largest potential for divergence as we argue here and show numerically in the following section.

Including the SpAMM error in the \tilde{z}_{k-1} update we have:

$$\begin{aligned}\tilde{z}_{k-1} &= \tilde{z}_{k-2} \otimes_{\tau} h_{\alpha}[\tilde{x}_{k-2}] \\ &= \Delta_{\tau} \tilde{z}_{k-2} \cdot h_{\alpha}[\tilde{x}_{k-2}] + \tilde{z}_{k-2} \cdot h_{\alpha}[\tilde{x}_{k-2}].\end{aligned}\quad (25)$$

Then, with $h_{\alpha}[\tilde{x}_{k-2}] = h_{\alpha}[x_{k-2}] + h'_{\alpha} \delta x_{k-2}$, and taking z_{k-1} from both sides, we find

$$\begin{aligned}\delta z_{k-1} &= \Delta_{\tau} \tilde{z}_{k-2} \cdot h_{\alpha}[\tilde{x}_{k-2}] \\ &\quad + \delta z_{k-2} \cdot h_{\alpha}[\tilde{x}_{k-2}] + z_{k-2} \cdot h'_{\alpha} \delta x_{k-2},\end{aligned}\quad (26)$$

which is bounded by

$$\begin{aligned}\delta z_{k-1} &< \|z_{k-2}\| (\tau \sigma_n \|h_{\alpha}[\tilde{x}_{k-2}]\| + h'_{\alpha} \delta y_{k-2} \|z_{k-2}\|) \\ &\quad + \delta z_{k-2} (\|h_{\alpha}[\tilde{x}_{k-2}]\| + \|y_{k-2}\|).\end{aligned}\quad (27)$$

In Eq. (27), the term $h'_{\alpha} \delta y_{k-2} \|z_{k-2}\|^2$ is volatile, tending towards $\delta y_{k-2} \kappa(s)/2$. Because of this sensitivity, and because the y_k product channel maintains fidelity of the starting eigen-basis, we single out this “sensitive” product for a higher level of precision; $\tau_s \ll \tau$. Still, we expect different behavior from the single instance $\tilde{y}_{k-1} = \tilde{z}_{k-1}^{\dagger} \otimes_{\tau_s} s$, and the dual instance $\tilde{y}_{k-1} = h_{\alpha}[\tilde{x}_{k-1}] \otimes_{\tau_s} \tilde{y}_{k-1}$. This is because the spectral product is broader (resolving larger and smaller numbers) in the single instance and narrower in the dual instance.

D. Most approximate but still stable

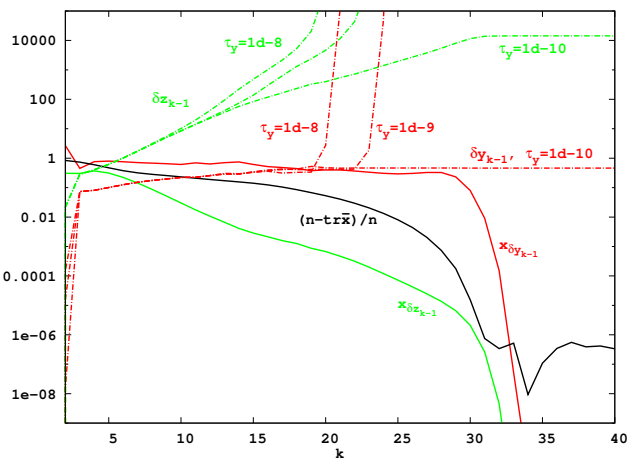


FIG. 2: Derivatives, displacements and trace error of the unscaled dual iteration. Derivatives are full lines, whilst the displacements cooresponding to $\tau_s = \{10^{-8}, 10^{-9}, 10^{-10}\}$ are the dashed lines. The trace error is shown as a full black line.

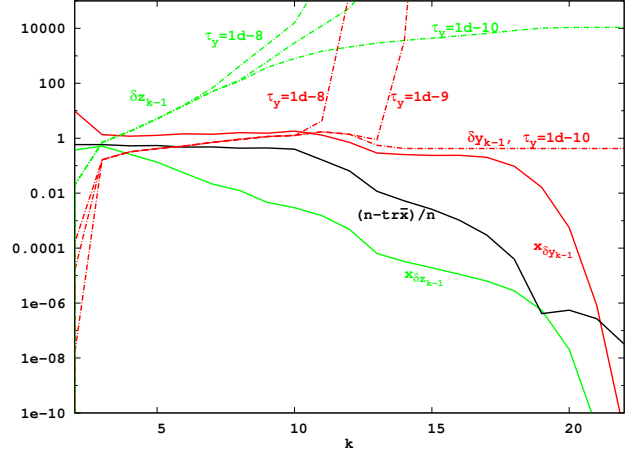


FIG. 3: Derivatives, displacements and the approximate trace of the scaled dual iteration. Derivatives are full lines, whilst the displacements cooresponding to $\tau_s = \{10^{-8}, 10^{-9}, 10^{-10}\}$ are the dashed lines. The trace error is shown as a full black line.

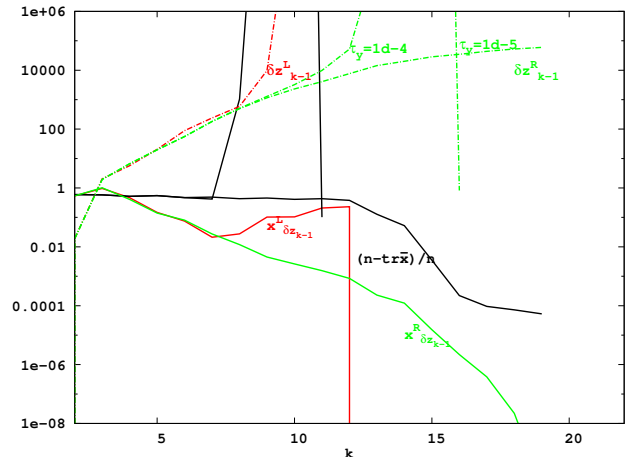


FIG. 4: Derivatives, displacements and the approximate trace of the scaled single iteration. Derivatives are full lines, whilst the displacements cooresponding to $\tau_s = \{10^{-3}, 10^{-4}, 10^{-5}\}$ are the dashed lines. The trace error is shown as a full black line.

Experiments were carried out on the ill-conditioned ($\kappa(s) = 10^{10}$) nanotube metric-matrices described in Appendix B. We picked $\tau = .001$ and block size $b = 64$. Then, we looked at stability with respect to the tighter τ_s threshold, the directional derivatives and the trace error.

In Fig. 2, unscaled results for the dual instance are shown. In Fig. 4, scaled results for the dual instance are given, recaining approximately 2/3 of the available $2\times$ acceleration, with a 1/3 penalty due to the stabilization map described in Section III C. Then, in Fig. ?? we show results for the scaled single instance.

Not shown is complete fillin at convergence for even

the most-approximate-yet-still-stable (MAYSS) value of τ_s . Also, with a less forgiving stability map, we find interesting left/right differences; namely, the right first product

$$\tilde{\mathbf{x}}_k^R \leftarrow \tilde{\mathbf{z}}_k^\dagger \otimes_\tau (\mathbf{s} \otimes_{\tau_s} \tilde{\mathbf{z}}_{k-1}) , \quad (28)$$

is different from the left first product

$$\tilde{\mathbf{x}}_k^L \leftarrow (\tilde{\mathbf{z}}_k^\dagger \otimes_{\tau_s} \mathbf{s}) \otimes_\tau \tilde{\mathbf{z}}_{k-1} , \quad (29)$$

which is unsurprising. The stability map parameters discussed Section III C are tuned away from such sensitivities, and their local variation has a negligible impact on stability. Also not shown, the intermediate volumes (before fill in) behave very differently with scaling; in all cases, the product volumes, proportional to the computational cost, are significantly increased by scaling. In the remainder of this work, we won't look at scaling again.

V. REGULARIZATION

Even for the most approximate but stable (MAYSS) approximations, our nanotube calculations become dense in both the data and task domains, even for very large $128 \times$ U.C. systems. For these ill-conditioned iterations, broad spectral resolutions that involving products of large and small numbers coorespond to delocalized products that are not tightly bound by the SpAMM approximation. However, as we show later in Fig. 12, similarly ill-conditioned problems may achieve substantial compression with just the MAYSS approximation.

A systematic way to reduce ill-conditioning is through Tikhonov regularization [1]. Regularization invokes a small level shift of the eigenvalues, $\mathbf{s}_\mu \leftarrow \mathbf{s} + \mu \mathbf{I}$, altering the condition number of the shifted matrix to $\kappa(\mathbf{s}_\mu) = \frac{\sqrt{s_{N-1}^2 + \mu^2}}{\sqrt{s_0^2 + \mu^2}}$.

Achieving substantial acceleration with severe ill-conditioning may require a large level shift however, producing inverse factors of little practical use. One approach to recover a more accurate inverse factor is Riley's method based on Taylor's series [2];

$$\mathbf{s}^{-1/2} = \mathbf{s}_\mu^{-1/2} \cdot \left(\mathbf{I} + \frac{\mu}{2} \mathbf{s}_\mu^{-1} + \frac{3\mu^2}{8} \mathbf{s}_\mu^{-2} + \dots \right) . \quad (30)$$

For severely ill-conditioned problems and large level shifts, this expansion may converge very slowly. Also, adding powers of the full inverse may not be computationally effective.

A. Product representation

We introduce an alternative representation of the regularized inverse factor;

$$\mathbf{s}^{-1/2} \equiv \bigotimes_{\substack{\tau=\tau_0 \\ \mu=\mu_0}} |\tau \mu ; \mathbf{s}^{-1/2}\rangle , \quad (31)$$

which is a telescoping product of preconditioned “slices” starting with a most-approximate-yet-still-effective-by-one-order (MAYEBOO) preconditioner, $\mathbf{s}_{\tau_0 \mu_0}^{-1/2} \equiv |\tau_0 \mu_0 ; \mathbf{s}^{-1/2}\rangle^1$. This sandwich of generic, thinly sliced SpAMM products allows to construct a nested scoping on precision via τ , and in the effective condition number controled by μ .

B. Effective by one order

We look again at the $\kappa(\mathbf{s}) = 10^{10}$ nanotube series described in Appendix B, this time with extreme regularization, $\mu_0 = .1$, and at a finer granularity, $b = 8$. Culled \mathbf{y}_k and \mathbf{z}_k volumes (as percentage of the total work) for $36 - 128 \times$ the (3,3) unit cell are shown for the MAYEBOO approximation in Fig. V B for the single instance, and in Fig. V B for the dual instance.

The behavior of these implementations is very different; in the single instance, a stable iteration could not be found at precision $\tau_0 = .1$. Stability could only be found at $\tau = 0.01$, and that with a poorly contained trace error and cull-volumes that continue to inflate past convergence. On the other hand, dual iteration volumes demonstrate collapsing volumes and fast trapping of the trace error with resolution of the approximate identity.

We interpret these results as follows: The single instance sufferes from an increasingly broad resolution of spectral powers, $\tilde{\mathbf{y}}_k \rightarrow \mathbf{s}_{\tau_0 \mu_0}^{-1/2} \otimes_{\tau_0} \mathbf{s}_{\mu_0}$, which is poorly bound by Eq. (5). In the dual instance however, $\tilde{\mathbf{y}}_k \rightarrow \mathbf{I}_{\tau_0 \mu_0} \otimes_{\tau_0} \mathbf{s}_{\tau_0 \mu_0}^{1/2}$ and $\tilde{\mathbf{z}}_k \rightarrow \mathbf{s}_{\tau_0 \mu_0}^{-1/2} \otimes_{\tau_0} \mathbf{I}_{\tau_0 \mu_0}$, with Eq. (5) tightening to

$$\Delta^{\mathbf{I}_{\tau_0 \mu_0} \cdot \mathbf{s}_{\tau_0 \mu_0}^{1/2}} < \tau n \|\mathbf{s}_{\tau_0 \mu_0}^{1/2}\| \quad (32)$$

and

$$\Delta^{\mathbf{s}_{\tau_0 \mu_0}^{-1/2} \cdot \mathbf{I}_{\tau_0 \mu_0}} < \tau n \|\mathbf{s}_{\tau_0 \mu_0}^{-1/2}\| . \quad (33)$$

This conctraction to the plane diagonal is compressive, leading to computational complexities that should approach quadtree copy in place.

C. Iterative regularization

We now sketch an iterative approach to constructing the product representation, Eq. (31). In the dual instance, it is possible to obtain a first MAYEBOO approximation $\mathbf{s}_{\tau_0=.1, \mu_0=.1}^{-1/2}$, that improves the condition number by one order of magnitude, with a numerical resolution of one digit. Then, a next level slice can be found, $\mathbf{s}_{\tau_0 \mu_1}^{-1/2}$,

¹ Braket notation marks the potential for assymetries in the intermediate representation.

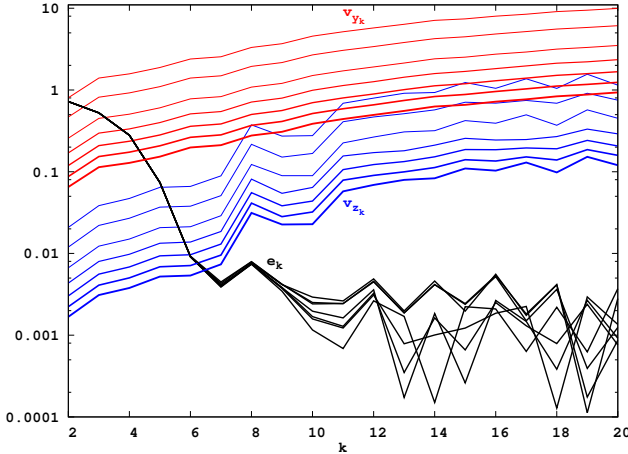


FIG. 5: Culled volumes in the thin slice, single instance approximation of $\mathbf{s}_{\tau_0 \mu_0}^{-1/2}$ for the (3,3) nanotube, $\kappa(\mathbf{s}) = 10^{10}$ matrix series described in Section B. In the “single” instance, it was not possible to achieve stability with $\tau_0 = .1$. In this “single” case, a thin slice corresponds to $\mu_0 = .1, \tau_0 = 10^{-2}$ & $\tau_s = 10^{-4}$, and volumes are $v_{\bar{z}_k} = (\text{vol}_{\bar{z}_{k-1} \otimes \tau_h[\bar{x}_{k-1}]}) \times 100\% / N^3$ and $v_{\bar{y}_k} = (\text{vol}_{\mathbf{s} \otimes \tau_s \bar{z}_k}) \times 100\% / N^3$. Line width increases with increasing system size. Also shown is the trace error, $e_k = (N - \text{tr } \mathbf{x}_k) / N$.

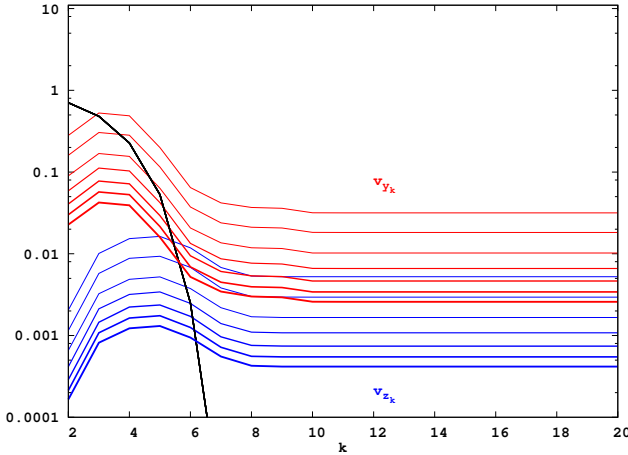


FIG. 6: Culled volumes in the thin slice, dual instance approximation of $\mathbf{s}_{\tau_0 \mu_0}^{-1/2}$ for the (3,3) nanotube, $\kappa(\mathbf{s}) = 10^{10}$ matrix series described in Section B. The thin slice corresponds to $\mu_0 = .1, \tau_0 = .1$ & $\tau_s = .001$ with volumes $v_{\bar{y}_k} = (\text{vol}_{h[\bar{x}_{k-1}] \otimes \tau_s \bar{y}_k}) \times 100\% / N^3$ and $v_{\bar{z}_k} = (\text{vol}_{\bar{z}_{k-1} \otimes \tau_h[\bar{x}_{k-1}]}) \times 100\% / N^3$. Line width increases with increasing system size. Also shown is the trace error, $e_k = (N - \text{tr } \mathbf{x}_k) / N$, which rapidly approaches 10^{-11} (not shown).

based on the residual $(\mathbf{s}_{\tau_0 \mu_0}^{-1/2})^\dagger \otimes_{\tau_1} (\mathbf{s} + \mu_1 \mathbf{I}) \otimes_{\tau_1} \mathbf{s}_{\tau_0 \mu_0}^{-1/2}$, with e.g. $\mu_1 = .01$ and $\tau_1 = .01$. The product $\mathbf{s}_{\tau_0 \mu_1}^{-1/2} \otimes_{\tau_1} \mathbf{s}_{\tau_0 \mu_0}^{-1/2}$ improves the condition number by two orders of magnitude, still with a numerical resolution of one digit. In preliminary work, it appears necessary to

compute the residual at a higher level of precision, e.g. using \otimes_{τ_1} instead of \otimes_{τ_0} and with $\tau_1 > \tau_0$.

In this way, it may be possible to obtain product representation of the inverse square root at a SpAMM resolution that is potentially far more permissive than otherwise possible,

$$\mathbf{s}_{\tau_0}^{-1/2} = \mathbf{s}_{\tau_0 \mu_n}^{-1/2} \otimes_{\tau_1} \mathbf{s}_{\tau_0 \mu_{n-1}}^{-1/2} \otimes_{\tau_1} \dots \mathbf{s}_{\tau_0 \mu_0}^{-1/2}, \quad (34)$$

assuming $.1 \geq \mu_0 > \mu_1 > \dots$. Likewise, it may also be possible to obtain the full inverse factor with increasing numerical resolution as

$$\mathbf{s}^{-1/2} = \mathbf{s}_{\tau_m}^{-1/2} \otimes_{\tau_{m+1}} \mathbf{s}_{\tau_{m-1}}^{-1/2} \otimes_{\tau_m} \dots \mathbf{s}_{\tau_0}^{-1/2}, \quad (35)$$

and $.1 \geq \tau_0 > \tau_1 > \dots$

With each step a well conditioned generic slice, it may be possible to find a more effective logistic map optimized for the corresponding eigenvalue distributions. Also, there are certainly other paths that can be taken in the scoping of regularization and precision that may be far more efficient. Finally, our sketch is vague about our ability to avoid forming the full product in application to a target vector or matrix.

As an example, we formalize the product representation (34) (a similar argument applies to (35) and (31)). To do so, let $\mu_0 > \mu_1 > \dots > \mu_j > 0$, and suppose that, for $j \geq 1$, R_{j-1} is the τ_0 approximation to $(S + \mu_{j-1} I)^{-1/2}$, so that

$$\left\| R_{j-1}^\dagger \otimes_{\tau_0} (S + \mu_{j-1} I) \otimes_{\tau_0} R_{j-1} - I \right\|_F \lesssim \tau_0.$$

Now let $S_{\tau_0, \mu_j}^{-1/2}$ denote a τ_0 approximation to $R_{j-1}^\dagger \otimes_{\tau_0} (S + \mu_j I) \otimes_{\tau_0} R_{j-1}$. It follows that $R_j = R_{j-1} \otimes_{\tau_0} S_{\tau_0, \mu_j}^{-1/2}$ is a τ_0 approximation to $(S + \mu_j I)^{-1/2}$. Indeed, by the stability of SpAMM (5),

$$\begin{aligned} \left(R_{j-1} \otimes_{\tau_0} S_{\tau_0, \mu_j}^{-1/2} \right)^\dagger &= \left(R_{j-1} S_{\tau_0, \mu_j}^{-1/2} \right)^\dagger + \mathcal{O}(\tau_0) \\ &= \left(S_{\tau_0, \mu_j}^{-1/2} \right)^\dagger (R_{j-1})^\dagger + \mathcal{O}(\tau_0) \\ &= \left(S_{\tau_0, \mu_j}^{-1/2} \right)^\dagger \otimes_{\tau_0} (R_{j-1})^\dagger + \mathcal{O}(\tau_0). \end{aligned}$$

Therefore,

$$\left\| R_j^\dagger \otimes_{\tau_0} (S + \mu_j I) \otimes_{\tau_0} R_j - I \right\|_F \lesssim \tau_0,$$

where R_j is given by the product representation

$$\begin{aligned} R_j &= R_{j-1} \otimes_{\tau_0} S_{\tau_0, \mu_j}^{-1/2} \\ &= R_{j-2} \otimes_{\tau_0} S_{\tau_0, \mu_{j-1}}^{-1/2} \otimes_{\tau_0} S_{\tau_0, \mu_j}^{-1/2} \\ &= S_{\tau_0, \mu_0}^{-1/2} \otimes_{\tau_0} \dots \otimes_{\tau_0} S_{\tau_0, \mu_{j-1}}^{-1/2} \otimes_{\tau_0} S_{\tau_0, \mu_j}^{-1/2}. \end{aligned}$$

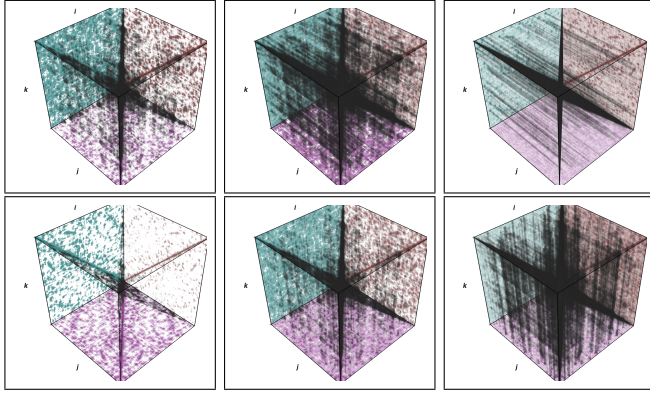


FIG. 7: The ijk task and data space for construction of the unregularized preconditioner $|\tau_0 = .001, \mu_0 = .0; s^{-1/2}\rangle$, with dual instance square root iteration, and for the 6-311G** metric of 100 periodic water molecules at STP. At top its $\mathbf{y}_k = h_\alpha[\mathbf{x}_{k-1}] \otimes \tau_s \mathbf{y}_{k-1}$ for $k = 0, 4, \& 15$, while on the bottom we have $\mathbf{x}_k = \mathbf{y}_k \otimes \tau_s \mathbf{z}_k$ for $k = 0, 4, \& 15$. Maroon is \mathbf{a} , purple is \mathbf{b} , green is \mathbf{c} , and black is the volume $\text{vol}_{\mathbf{a} \otimes \tau_s \mathbf{b}}$ in the product $\mathbf{c} = \mathbf{a} \otimes \tau_s \mathbf{b}$.

VI. LOCALITY

A. Spatial, metric and temporal locality

Astrophysical n -body algorithms employ range queries over spatial databases to hierarchically discover and compute approximations that commit only small errors. Often, these spatial databases are ordered with a space filling curve (SFC) [], which maps points that are close in space to an index where they are also close. The block-by-magnitude structures empowering the SpAMM approximation are metric localities cooresponding to metric decay, in quantum chemical examples cooresponding to an underlying SFC ordering of Cartesian coordinates.

Warren and Salmon showed how to parlay spatial locality into temporal locality, remapping and repartitioning the space filling curve to rebalance distributed n -body tasks, based on accumulated histories (persistence data). In a similar way, we showed how persistence can be used to achieve strong parallel scaling for SpAMM with commonly available runtimes []. Persistence data, providing temporal locality, may also be useful in mathematical approximation.

In Figure 7, we show \otimes_τ volumes for square root iteration, cooresponding to the metric of a small, periodic water box with the large 6-311G** basis (Appendix B). For the 3-d periodic case, diminishing Cartesian separations lead to long-skinny delocalizations (pillae) and much denser matrices, relative to e.g. a one-dimensional nano-tube.

These delocalizations coorespond to weakness in Eq. (5), and to the tighter thresholds required to maintain a single iteration in the MAYSS approximation. This effect is even more pronounced in the single instance (not shown), where delocalizations are exaggerated due to spec-

tral resolutions that are broader. Eventually, Cartesian seperation will thin the density of these delocalizations, with complexity reduction due to metric seperation and decay only. However, this may be painfully slow.

B. Algebraic locality

In Figures 8 and 9, we show a new kind of locality that is uniquely exploited by n -body approximation of the square root iteration. This locality increases compressively towards convergence, as the contractive identity iteration develops. We call this compression ***lensing***, involving collapse of the culled volume about plane diagonals of the resolvent. Lensing cooresponds to strengthening Eq.(5), and strongly contracting directional derivatives, Eqs. (22)-(23). This is an important, mitigating computational effect for the sensitive \mathbf{y}_k channel, with $\tau_s \sim .01 \times \tau$.

In addition, non-Euclidian measures are relevent for achieving metric locality in the SpAMM algebra, including information measures, space filling curve generalizations, as well as graph reorderings that band matrix elements about the diagonal [], a common approach in structural mechanics. In Figure 12 we show development of a first, unregularized (MAYSS) preconditioner for such an example; the structural matrix $\mathbf{s} = \text{bcsstk14}$ is a $\kappa(\mathbf{s}) = 10^{10}$ matrix cooresponding to the roof of the Omni Coliseum in Atlanta []. These results show remarkable gossamer sheeting and flattening along plane diagonals, at top for developmentent of \mathbf{y}_k , as well as hollow accumulation of $\text{vol}_{\mathbf{y}_k \otimes \tau_s \mathbf{z}_k}$. Surprisingly, this example demonstates lensing for a tight MAYSS approximation, while the equally ill-conditioned & lower dimensional $\kappa(\mathbf{s}) = 10^{10}$ nanotube MAYSS approximation remains full (dense) through U.C. $\times 128$.

C. Complexity reduction

Finally, we show complexity reduction at convergence of the MAYEBOO approximation relative to the MAYSS approximation, in Fig. 10 for periodic water boxes, and in Fig. 11 for the ill-conditioned nano-tube. The two-orders difference between \mathbf{y}_k and \mathbf{z}_k volumes cooresponds precisely to $\tau_s \sim \tau \times .01$, with \mathbf{x}_k in between. Except for the slower trend in Fig. (10)'s \mathbf{x}_k volume, we see the potential for continued strong acceleration with increasing system size. Understanding these subtlties is the subject of future work.

VII. CONCLUSIONS

In this work, we developed the n -body solver SpAMM for square root iteration. Main contributions include a modified Cauchy-Schwarz criterion, Eq. ??, and proof that the cooresponding relative product error is bound by

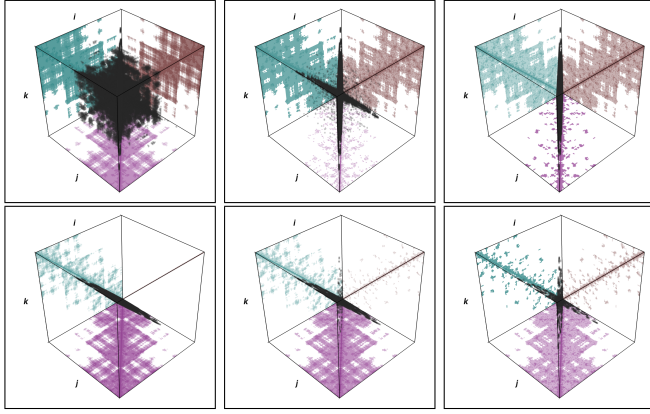


FIG. 8: The ijk task and data space for construction of the MAYEBOO preconditioner $|\tau_0 = .1, \mu_0 = .1; s^{-1/2}\rangle$, with dual instance square root iteration, and for an $8 \times$ U.C. (3,3) $\kappa(s) = 10^{11}$ nanotube. \mathbf{y}_k appears wider than \mathbf{z}_k because it is computed at a higher precision, $\tau_s = .001$, and because the first multiply involves s^2 . At top its $\mathbf{y}_k = h_\alpha[\mathbf{x}_{k-1}] \otimes_{\tau_s} \mathbf{y}_{k-1}$ for $k = 0, 4, \& 16$, while on the bottom we have $\mathbf{x}_k = \mathbf{y}_k \otimes_{\tau} \mathbf{z}_k$ for $k = 0, 2, \& 16$. Maroon is \mathbf{a} , purple is \mathbf{b} , green is \mathbf{c} , and black is the volume $\text{vol}_{a \otimes_{\tau} b}$ in the product $\mathbf{c} = \mathbf{a} \otimes_{\tau} \mathbf{b}$.

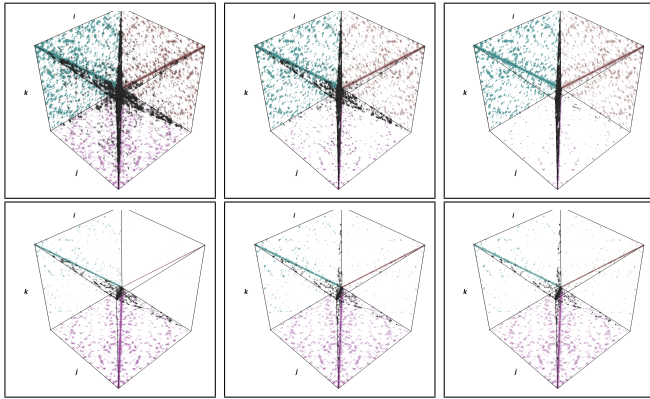


FIG. 9: The ijk task and data space for construction of the MAYEBOO preconditioner $|\tau_0 = .1, \mu_0 = .1; s^{-1/2}\rangle$, with dual instance square root iteration and for 6-311G** metric of 100 periodic water molecules at STP. At top its $\mathbf{y}_k = h_\alpha[\mathbf{x}_{k-1}] \otimes_{\tau_s} \mathbf{y}_{k-1}$ for $k = 0, 4, \& 15$, while on the bottom we have $\mathbf{x}_k = \mathbf{y}_k \otimes_{\tau} \mathbf{z}_k$ for $k = 0, 4, \& 15$. Maroon is \mathbf{a} , purple is \mathbf{b} , green is \mathbf{c} , and black is the volume $\text{vol}_{a \otimes_{\tau} b}$ in the product $\mathbf{c} = \mathbf{a} \otimes_{\tau} \mathbf{b}$.

Eq. (5). Also, we demonstrated a new kind of algebraic locality, lensing, that develops with strongly contractive identity iteration.

This work is gauged against other methods for fast matrix multiplication discussed in Section ???. Against SpGEMM, the n -body approach offers a bounded control over relative errors in the product and the ability to resolve complex algebraic structures, about plane-diagonals of the ijk -cube, along tall-skinny pillae and for volumetric contractions to lower dimensional objects via lensing. The n -body method uniquely and synergistically exploits two distinct forms of locality, metric local-

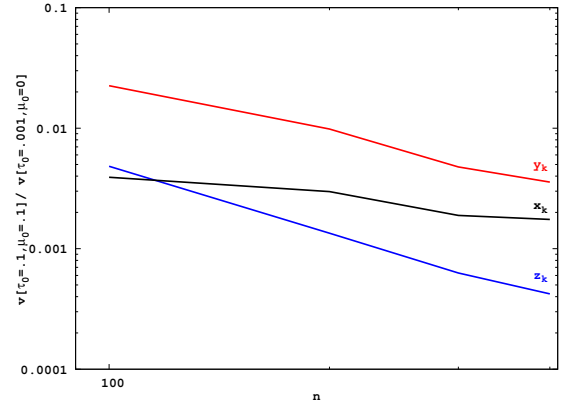


FIG. 10: Complexity reduction in metric square root iteration for periodic 6-311G** water. Shown is the ratio of lensed product volumes for the regularized most-approximate-yet-effective-by-one-order (MAYEBOO) approximation and the unregularized most-approximate-yet-still-stable (MAYSS) approximation.

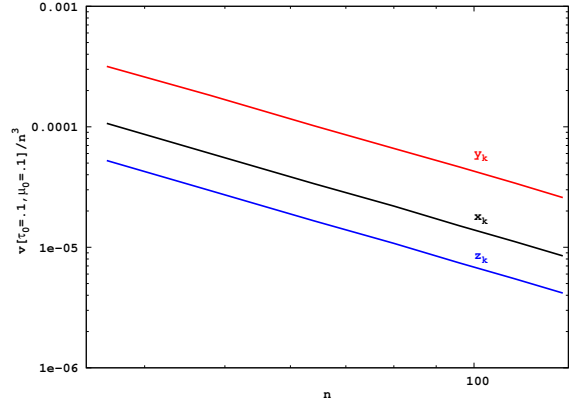


FIG. 11: Complexity reduction in metric square root iteration for periodic 6-311G** water. Shown is the ratio of lensed product volumes for the regularized most-approximate-yet-effective-by-one-order (MAYEBOO) approximation and the unregularized most-approximate-yet-still-stable (MAYSS) approximation.

ity cooresponding to a Cartesian or non-Euclidean decay principle, and algebraic locality cooresponding to contractive identity iteration. Also, strong parallel scaling for the $\mathcal{O}(n)$ electronic structure problem has been demonstrated with the SpAMM kernel, a feature that remains elusive for methods based on SpMM [?].

Against methods for matrix compression [], as well as against Fast Matrix Multiplication of the Strassen type [], the quadtree data structure and the octree task space employed by SpAMM are complimentary. Likewise in the case of sketch products [], it might be possible to deploy streaming approaches for these tall-skinny delocalizations under certain conditions []. Thus, the concurrent application of fast methods for matrix multiplication may be enabled by the database framework supporting n -body

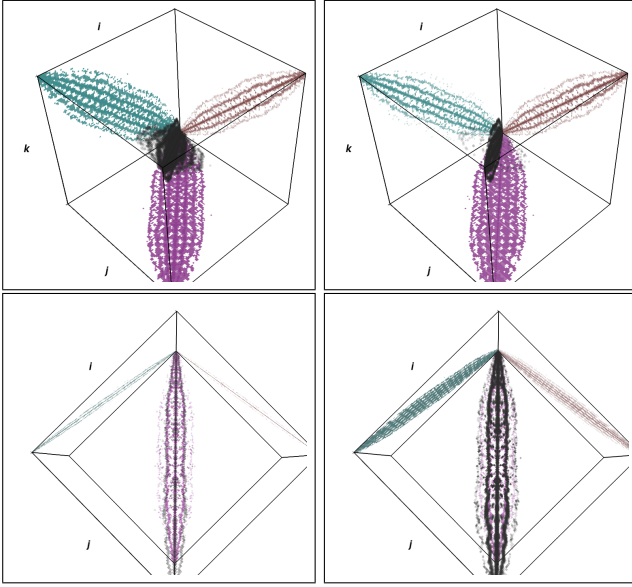


FIG. 12: The ijk task and data space for construction of the unregularized preconditioner $|\tau_0 = .001, \mu_0 = .0; s^{-1/2}\rangle$, with the dual instance of square root iteration and for 6-311G** metric of 100 periodic water molecules at STP. At top its $\mathbf{y}_k = h_\alpha[\mathbf{x}_{k-1}] \otimes_{\tau_s} \mathbf{y}_{k-1}$ for $k = 0, 4, \& 15$, while on the bottom we have $\mathbf{x}_k = \mathbf{y}_k \otimes_{\tau_s} \mathbf{z}_k$ for $k = 0, 4, \& 15$. Maroon is \mathbf{a} , purple is \mathbf{b} , green is \mathbf{c} , and black is the volume $\text{vol}_{\mathbf{a} \otimes_{\tau_s} \mathbf{b}}$ in the product $\mathbf{c} = \mathbf{a} \otimes_{\tau_s} \mathbf{b}$.

approximations.

Beyond the fast matrix multiply, n -body frameworks may enable additional, layered functionalities and economizations in complex solver ecosystems, with facile interoperability and mathematical agility, through generic recursion and skelitization, and with common runtimes able to exploit temporal and data localities. For example, we recently generalized SpAMM recursion to the problem of Fock-exchange, with a recursive triple (hextree) metric query on the Almlöf-Alhrichs direct SCF criteria []. Also, mathematical equivalence with the matrix sign function, Eq. (??), and close structural relationships with

the polar decomposition may enable to extend functionality of the n -body iterations developed here.

Despite these compelling qualities, n -body square-root iteration must be gauged by its ability to compute a high quality inverse factor. Here, we have only looked at complexity and stability of the most approximate preconditioners for a few systems and for a few numerical experiments. However, the results are new and encouraging, showing the potential for many orders of magnitude reduction in complexity.

Appendix A: Implementation

FP, F08, OpenMP 4.0 In the current implementation, all persistence data (norms, flops, branches & etc.) are accumulated compactly in the backward recurrence. This persistence data that may be achieved by minimal locally essential trees [].

For these reasons, maintaining connection to the eigenvectors of \mathbf{s} through a tighter first product is necessary. In the single instance, and with a tighter “ s ” product, $\tau_s \ll \tau$, we find very interesting left/right differences; namely, the right first product

$$\tilde{\mathbf{x}}_k^R \leftarrow \tilde{\mathbf{z}}_k^\dagger \otimes_{\tau_s} (\mathbf{s} \otimes_{\tau_s} \tilde{\mathbf{z}}_{k-1}) , \quad (\text{A1})$$

is different from the left first product

$$\tilde{\mathbf{x}}_k^L \leftarrow (\tilde{\mathbf{z}}_k^\dagger \otimes_{\tau_s} \mathbf{s}) \otimes_{\tau_s} \tilde{\mathbf{z}}_{k-1} . \quad (\text{A2})$$

damping the inversion and the small value to be added c is called Marquardt-Levenberg coefficient

Map switching and etc based on TrX

Appendix B: Data

3,3 carbon nanotube with diffuse sp -function double exponential (Fig.)

-
- [1] O. Penrose and J. Lebowitz, Commun. Math. Phys. **184** (1974).
 - [2] J. Voit, *The Statistical Mechanics of Financial Markets*, Theoretical and Mathematical Physics (Springer Berlin Heidelberg, 2006), ISBN 9783540262893, URL <https://books.google.com/books?id=6zUlh\TkWSwC>.
 - [3] L. Anselin, Int. Reg. Sci. Rev. **26**, 153 (2003), ISSN 01600176, URL <http://irx.sagepub.com/cgi/doi/10.1177/0160017602250972>.
 - [4] J. Hardin, S. R. Garcia, and D. Golan, Ann. Appl. Stat. **7**, 1733 (2013), ISSN 1932-6157, arXiv:1106.5834v4.
 - [5] I. Krishtal, T. Strohmer, and T. Wertz, Found. Comput. ... (2013), ISSN 1615-3375.
 - [6] P. O. Lowdin, Advances in Physics **5**, 1 (1956).
 - [7] A. R. Naidu, p. 1 (2011), 1105.3571.
 - [8] N. J. Higham, *Functions of Matrices* (Society for Industrial & Applied Mathematics,, 2008).
 - [9] F. G. Gustavson, ACM Transactions on Mathematical Software (TOMS) **4**, 250 (1978).
 - [10] S. Toledo, IBM J. Res. Dev. **41**, 711 (1997).
 - [11] M. Challacombe, Comput. Phys. Commun. **128**, 93 (2000).
 - [12] D. R. Bowler and T. M. and M. J. Gillan, Comp. Phys. Comm. **137**, 255 (2000).
 - [13] M. Benzi and M. Tuma, Appl. Numer. Math. **30**, 305 (1999).
 - [14] M. Benzi, J. Comput. Phys. **182**, 418 (2002).
 - [15] D. R. Bowler and T. Miyazaki, Reports Prog. Phys. **75**, 36503 (2012).
 - [16] M. Benzi, P. Boito, and N. Razouk, SIAM Rev. **55**, 3

- (2013).
- [17] V. Strassen, Numer. Math. **13**, 354 (1969).
 - [18] G. Ballard, J. Demmel, O. Holtz, and O. Schwartz, Communications of the ACM **57**, 107 (2014).
 - [19] A. G. Gray and A. W. Moore, in *Advances in Neural Information Processing Systems* (MIT Press, 2001), vol. 4, pp. 521–527, URL <http://citesearx.ist.psu.edu/viewdoc/summary?doi=10.1.1.28.7138>.
 - [20] A. Gray (2003), URL <http://reports-archive.adm.cs.cmu.edu/anon/anon/2003/abstracts/03-222.html>.
 - [21] T. Sarlos, In Proceedings of the 47th Annual IEEE Symposium on Foundations of Computer Science (FOCS) (2006).
 - [22] P. Drineas, R. Kannan, and M. W. Mahoney, SIAM Journal on Computing **36**, 132 (2006).
 - [23] M. W. Mahoney, pp. 1–53 (2012), arXiv:1502.03032v1.
 - [24] R. Pagh, ACM Trans. Comput. Theory **5**, 1 (2013).
 - [25] J. V. T. Sivertsen (2014).
 - [26] D. P. Woodruff, **10**, 1 (2015), arXiv:1411.4357v3.
 - [27] P. Mishra and M. H. Eich, ACM Comput. Surv. **24**, 63 (1992).
 - [28] E. G. Hoel and H. Samet, in *Parallel Processing, 1994. ICPP 1994. International Conference on* (1994), vol. 3, pp. 227–234.
 - [29] E. H. Jacox and H. Samet, ACM Trans. Database Syst. **28**, 230 (2003).
 - [30] S. Chen, A. Ailamaki, P. B. Gibbons, and T. C. Mowry, ACM Trans. Database Syst. **32** (2007).
 - [31] R. R. Amossen and R. Pagh, in *Proceedings of the 12th International Conference on Database Theory* (ACM, 2009), pp. 121–126.
 - [32] M. D. Lieberman, J. Sankaranarayanan, and H. Samet, in *Proceedings of the 2008 IEEE 24th International Conference on Data Engineering* (IEEE Computer Society, Washington, DC, USA, 2008), pp. 1111–1120, ISBN 978-1-4244-1836-7.
 - [33] C. Kim, T. Kaldewey, V. W. Lee, E. Sedlar, A. D. Nguyen, N. Satish, J. Chhugani, A. Di Blas, and P. Dubey, Proc. VLDB Endow. **2**, 1378 (2009).
 - [34] Z. Bai and J. Demmel, SIAM J. Matrix Anal. Appl. **19**, 205 (1998).
 - [35] N. J. . Higham, N. M. D . Steven Mackey, and F. . coise Tisseur, SIAM J. Matrix Anal. Appl. **26**, 849 (2005).
 - [36] J. Chen and E. Chow, Preprint ANL/MCS-P5059-0114, Mathematics and Computer Science Division, Argonne National Laboratory, Argonne, IL 60439 (2014).
 - [37] V. Pan and R. Schreiber, SIAM J. Sci. Stat. Comput. (1991).